

## DETERMINING THE HOT-DEFORMATION CHARACTERISTICS OF A 1235 ALUMINUM ALLOY USING A PROCESSING MAP

### ZNAČILNOSTI VROČE DEFORMACIJE ALUMINIJEVE ZLITINE 1235 Z UPORABO NAČRTA PROCESIRANJA

Wenduan Yan<sup>1,2</sup>, Gaosheng Fu<sup>1</sup>

<sup>1</sup>College of Materials Science and Engineering, Fuzhou University, Fuzhou 350108, China

<sup>2</sup>Fujian Chuanzheng Communications College, Fuzhou 350007, China  
fugaosheng@fzu.edu.cn

*Prejem rokopisa – received: 2012-06-01; sprejem za objavo – accepted for publication: 2012-07-13*

A hot-processing map and TEM images of a 1235 aluminum alloy have been used while studying hot-deformation characteristics of this alloy. The results showed that an ideal processing region exists in the high-temperature/low-strain-rate area and that the power-dissipation efficiency is around 46 %. It is better to avoid deformations at the low-temperature/high-strain rate and the high-temperature/moderate-strain rate due to their processing instability and lower power-dissipation efficiency.

Keywords: 1235 aluminum alloy, processing map, hot deformation, dynamic recrystallization

Načrt vročega preoblikovanja in TEM-posnetki aluminijeve zlitine 1235 so bili uporabljeni pri študiju značilnosti preoblikovanja v vročem aluminijeve zlitine 1235. Rezultati so pokazali, da obstaja idealno področje preoblikovanja v območju visoke temperature – majhne preoblikovalne hitrosti in z okrog 46 % izgube učinkovite moči. Boljše se je izogibati preoblikovanju pri nizkih temperaturah – velikih preoblikovalnih hitrostih in pri visokih temperaturah – zmernih preoblikovalnih hitrostih zaradi nestabilnosti preoblikovanja in manjše učinkovitosti izgubljene moči.

Ključne besede: aluminijeva zlitina 1235, načrt preoblikovanja, deformacija v vročem, dinamična rekristalizacija

## 1 INTRODUCTION

A processing map is regarded as a good method for analyzing the workability of a metal. The map describes not only a particular deformation mechanism of a microstructure in a certain region, but also that in an uncertain region that should be avoided in processing.<sup>1,2</sup> The 1235 aluminum stock is mainly used for cigarette foils, aluminum-foil containers and cooking bags; all of these have the advantages of innocuity, health, high flexibility, moisture resistance, etc.<sup>3</sup> So far only a small amount of research on the complicated deformation process of aluminum alloys has been conducted due to their poor flowability and sensitivity to the temperature and strain rate. It is important to study the deformation characteristics of the 1235 aluminum alloy for optimizing the processing performance and controlling the internal microstructure evolution using a processing map. Studying this phenomenon is of theoretical significance and practical value in a hot-processing analysis and design.

## 2 THEORY

The processing map is developed on the basis of the dynamic-materials mode (DMM).<sup>4</sup> The basis for and principles of this approach have been described earlier and its applications to hot working in a wide range of

alloys have been compiled.<sup>5</sup> According to the model, a workpiece undergoing hot deformation can be considered as a dissipater of power. The total power  $P$  may be divided into two complementary functions:  $G$  content and  $J$  co-content:

$$P = \sigma \cdot \dot{\epsilon} = G + J = \int_0^i \sigma \cdot d\dot{\epsilon} + \int_0^{\sigma} \dot{\epsilon} \cdot d\sigma \quad (1)$$

where  $\sigma$  is the stress of the alloy during hot deformation, and  $\dot{\epsilon}$  is the strain rate. The  $G$  dissipater content represents the power dissipated by plastic deformation, most of which is converted to viscoplastic heat. The  $J$  dissipater co-content represents the power dissipation through metallurgical changes. The power partitioning between  $G$  and  $J$  is controlled by the constitutive flow behavior of the material and is decided by the strain-rate sensitivity ( $m$ ):

$$\frac{dJ}{dG} = \frac{\dot{\epsilon} ds}{\sigma d\dot{\epsilon}} = \frac{d \ln \sigma}{d \ln \dot{\epsilon}} = m \quad (2)$$

The dynamic constitutive equation can be expressed like this:

$$\sigma = K \dot{\epsilon}^m \quad (3)$$

In equation (3) symbol  $K$  represents a constant. At any given deformation temperature,  $J$  is evaluated by the integrating equation (3) and the power dissipated in changing the microstructure is given by the following:

$$J = P - G = \sigma \dot{\epsilon} \int_0^i K \dot{\epsilon}^m \cdot d\dot{\epsilon} = \frac{m}{m+1} \sigma \dot{\epsilon} \quad (4)$$

where  $m$  represents the strain-rate sensitivity. For an ideal linear dissipater,  $m = 1$  and  $J = J_{max} = \sigma \dot{\epsilon} / 2$ . The efficiency of the power dissipation of linear dissipater may be expressed as a dimensionless parameter:

$$\eta = \frac{J}{J_{max}} = \frac{m}{m+1} \quad (5)$$

The variation of  $\eta$  with the temperature and strain rate constitutes the power-dissipation map. Various domains in the power-dissipation map may be correlated with specific microstructural mechanisms.

The continuum-instability criterion based on the extreme principles of irreversible thermodynamics as applied to the large plastic flow is used in this study to identify the regimes of flow instabilities.<sup>6</sup> The principle of the maximum rate of the entropy production in a metallurgical system results in an instability criterion given by:

$$\xi(\dot{\epsilon}) = \frac{\partial \ln \left( \frac{m}{m+1} \right)}{\partial \ln \dot{\epsilon}} + m < 0 \quad (6)$$

The variation of the instability parameter  $\xi(\dot{\epsilon})$  at different temperatures and strain rates constitutes an instability map.

Finally, a processing map is built by superimposing an instability map on a power-dissipation map. From a processing map, metal-working processes can be designed and controlled for good workability and desired microstructure.<sup>7</sup>

### 3 EXPERIMENTS

Aluminum alloys used in this investigation were melted with high-efficiency purification,<sup>8-10</sup> and the percentage of the inclusions tested with flux irrigation was 0.051 %. The chemical composition (in mass fractions, w/%) is shown in **Table 1**. Ingots were dealt with homogenizing annealing under the conditions of an annealing temperature of 833 K for 13 h, and were air-cooled.<sup>11</sup>

After the homogenizing annealing, the 1235 aluminum alloy was machined into cylindrical specimens with a diameter of 10 mm and a height of 12 mm. Isothermal, axisymmetric compression tests were held in a Geeble-1500 dynamic, thermal/mechanical simulation machine under the conditions of a deformation temperature of 573–773 K, a strain rate of 0.01–10 s<sup>-1</sup>, and a

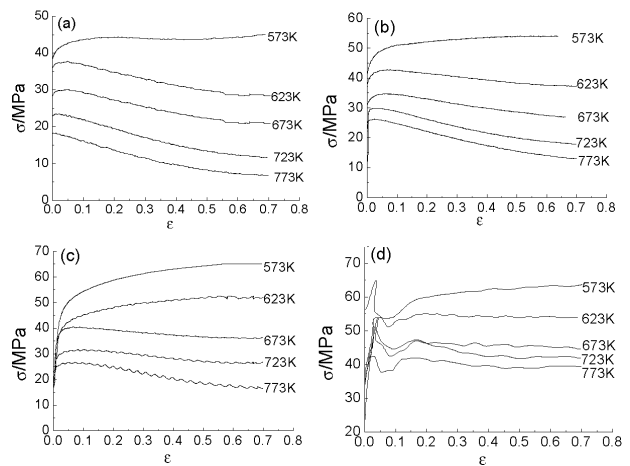


**Figure 1:** True stress-strain curves of the 1235 aluminum alloy: a) 0.01 s<sup>-1</sup>, b) 0.1 s<sup>-1</sup>, c) 1.0 s<sup>-1</sup> and d) 10.0 s<sup>-1</sup>

**Slika 1:** Krivulje tečenja aluminijeve zlitine 1235: a) 0,01 s<sup>-1</sup>, b) 0,1 s<sup>-1</sup>, c) 1,0 s<sup>-1</sup> in d) 10,0 s<sup>-1</sup>

deflection of 50 %. All specimens were cooled rapidly with water to keep the dynamically recrystallized microstructure. The true stress-strain curves obtained from the hot-deformation experiments are shown in **Figure 1**. The deformed specimens were sectioned parallel to the compression axis and the microstructure was determined using transmission electron microscopy (TEM) of the Tecnai GZ F20 S-Twin model.

According to **Figure 1**, the hot-working character of the 1235 aluminum alloy is obvious. At the strain rates less than 10 s<sup>-1</sup>, work hardening followed by dynamic softening appears with increasing strain, then it shows a steady-state flow characteristic when the strain is bigger than 0.4. At a high strain rate of 10.0 s<sup>-1</sup> (**Figure 1d**) the flow stress reaches an initial peak and this is followed by rapid softening. With the increasing strain, the stress remains unchanged and shows the steady-state flow characteristic, which is appropriate in the building of a hot-processing map.

### 4 RESULTS AND DISCUSSION

#### 4.1 Power-dissipation map

A higher power-dissipation efficiency allows better metal processability.<sup>5,6</sup> Strain-rate sensitivity  $m$  at different deformation temperatures and strain rates should be calculated first when building a power-dissipation map. The power-dissipation map of the 1235 aluminum alloy at different strains was built using the flow stress (**Figure 1**) obtained from the hot-compression tests. In order to make the values more reliable,

**Table 1:** Chemical composition of the 1235 aluminum alloy

**Tabela 1:** Kemijska sestava aluminijeve zlitine 1235

Element	Si	Fe	Cu	Mn	Mg	Ni	Zn	Ti	Al
Composition, w/%	0.095	0.38	0.002	0.002	0.0001	0.0001	0.006	0.015	balance

we used the cubic-spline function to interpolate  $\lg \sigma$  and  $1/T$ , and obtained more flow-stress values at other temperatures. The results of the cubic-spline curves of  $\lg \sigma$  and  $1/T$  at a strain of 0.7 are shown in **Figure 2**. The points in the figure stand for the values of the flow stress, respectively. Based on the fitted spline curve, the flow-stress values can be drawn at different deformation temperatures. More points or fewer points in the map should not be used to reduce the computation or to ensure the accuracy of the data. From the stress values corresponding to the five experimental temperatures, the values of the flow stress corresponding to the other middle temperature of the four temperatures were obtained, that is, the stress values at the temperatures of 598 K, 648 K, 698 K and 748 K. On the basis of equation (2), we fitted the curves of  $\lg \sigma$  and  $\lg \dot{\epsilon}$  with the cubic-spline function getting the slope that is called the strain-rate sensitivity  $m$ . **Figure 3** shows the cubic-spline

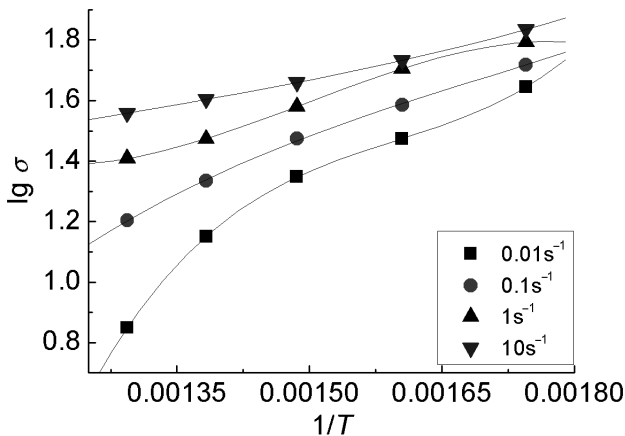


**Figure 2:** Cubic-spline curves of  $\lg \sigma$  and  $1/T$  of the 1235 aluminum alloy at different strain rates  
**Slika 2:** Krivulje  $\lg \sigma$  in  $1/T$  za aluminijevo zlitino 1235 pri različnih hitrostih preoblikovanja

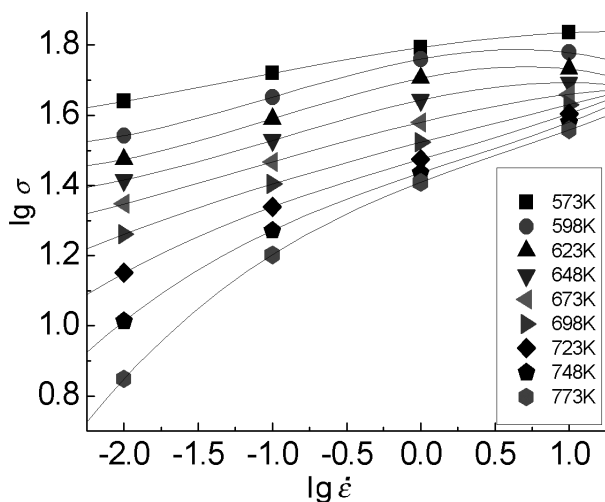


**Figure 3:** Cubic-spline curves of  $\lg \sigma$  and  $\lg \dot{\epsilon}$  of the 1235 aluminum alloy at different deformation temperatures  
**Slika 3:** Krivulje  $\lg \sigma$  in  $\lg \dot{\epsilon}$  za aluminijevo zlitino 1235 pri različnih temperaturah deformacije

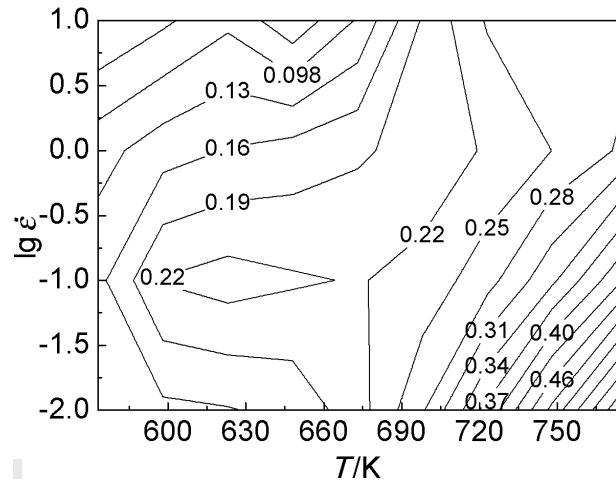


**Figure 4:** Power-dissipation map of the 1235 aluminum alloy  
**Slika 4:** Načrt izgube moči za aluminijevo zlitino 1235

curves of  $\lg \sigma$  and  $\lg \dot{\epsilon}$  at the strain of 0.7 in the 1235 aluminum alloy. From the material dynamic constitutive equation (3), the derivative of spline curves is the strain-rate sensitivity  $m$ .

The power-dissipation-efficiency factor  $\eta$  caused by the changes in the microstructure can be obtained from equation (5) after getting the strain-rate sensitivity  $m$  at different strains and strain rates. Finally, we drew the equivalent profile curve of the power-dissipation-efficiency factor  $\eta$  in the plane of  $\lg \dot{\epsilon} - T$  and got the power-dissipation map at the strain of 0.7.

**Figure 4** shows the power-dissipation map of the 1235 aluminum alloy at the strain of 0.7.

The contour line in **Figure 4** has the same power-dissipation efficiency. Figures on the lines are the values of the power-dissipation efficiency  $\eta$  corresponding to the deformation conditions. The contour lines, known as the loci of the microstructure, correspond to specific organizations indicating the changes in the microstructure during the hot deformation. The region of the highest-power dissipation is considered as the best processing-performance zone.<sup>12</sup> As seen in **Figure 4**, the power-dissipation efficiency  $\eta$  of the 1235 aluminum alloy increases from the upper left-hand corner to the lower right-hand corner. The maximum value of the power-dissipation efficiency  $\eta$  of the 1235 aluminum alloy is more than 46 % in the region of 773 K and 0.01 s<sup>-1</sup>, while its minimum value is only 9.8 % in the region of 573 K and 10.0 s<sup>-1</sup>. This indicates that the dissipation efficiency increases from the low-temperature/high-strain-rate region to the high-temperature/low-strain-rate region with regard to the microstructure evolution. The efficiency of the microstructure evolution reaches its maximum at 773 K and 0.01 s<sup>-1</sup>.

#### 4.2 Instability map

Hot-processing-instability map can be used for determining the best processing area and the instability

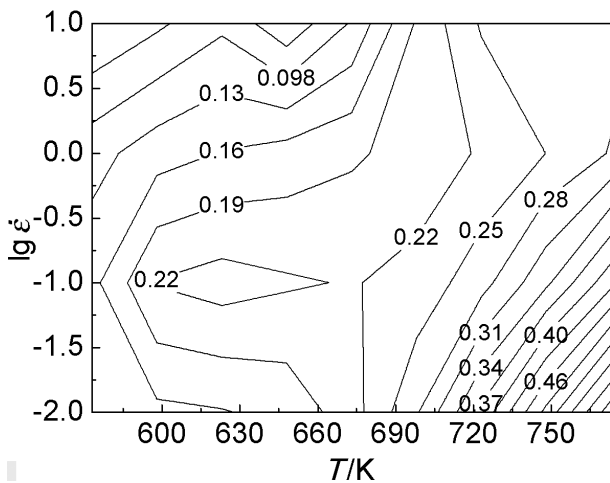


**Figure 5:** Cubic-spline curves of  $\lg [m/(m + 1)]$  and  $\lg \dot{\epsilon}$  of the 1235 aluminum alloy  
**Slika 5:** Krivulje  $\lg [m/(m + 1)]$  in  $\lg \dot{\epsilon}$  za aluminijevo zlitino 1235

area of a metal. First we calculated the value of  $\lg [m/(m + 1)]$  from the value of the strain-rate-sensitivity index  $m$  at the strain of 0.7 under each deformation temperature, then we fitted the curve of  $\lg [m/(m + 1)]$  and  $\lg \dot{\epsilon}$  with the cubic-spline function. After that, the value of  $\xi(\dot{\epsilon})$  in equation (6) was obtained by adding the slope of the spline function to the strain-rate-sensitivity value  $m$  which had been acquired before. The cubic-spline curves of  $\lg [m/(m + 1)]$  and  $\lg \dot{\epsilon}$  of the 1235 aluminum alloy at the strain of 0.7 are shown in **Figure 5**.

The hot-processing-instability map at the strain of 0.7 can be obtained by plotting the region of  $\xi(\dot{\epsilon}) < 0$  in the  $\lg \dot{\epsilon} - T$  plane. **Figure 6** shows the hot-processing-instability map of the 1235 aluminum alloy.

Materials processing in the region of  $\xi(\dot{\epsilon}) < 0$  may turn out to be unstable. As seen in **Figure 6**, the instability area appears in the low-temperature/high-strain-rate region and the high-temperature/moderate-strain-rate region. At the low-temperature/high-strain

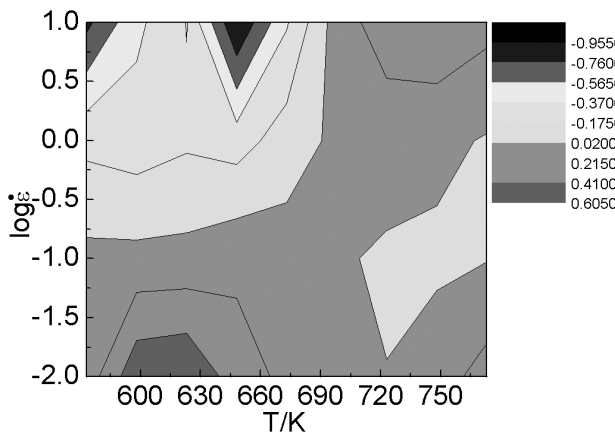


**Figure 6:** Hot-processing-instability map of the 1235 aluminum alloy  
**Slika 6:** Načrt nestabilnega preoblikovanja v vročem za aluminijevo zlitino 1235

rate, the material is prone to adiabatic shear band or local flow and reveals instability. At the high-temperature/moderate-strain rate, the dynamic recrystallization softening is not consistent with the hardening in some cases, thus causing a local strain or flow instability. As a result, this affects the deformed microstructure and its mechanical property. The material is more stable at the low-deformation-temperature/low-strain rate. However, the region of  $\xi(\dot{\epsilon}) < 0$  does not fully correspond with the actual instability region due to an inaccuracy in the calculation. Therefore, it is prone to instability in the darker region.

**4.3 Hot-processing map**

The hot-processing map of the 1235 aluminum alloy can be obtained by overlapping both the power-dissipation map and the instability map. **Figure 7** shows the hot-processing map of the 1235 aluminum alloy.

The highest power dissipation is considered to have the best processing performance.<sup>12</sup> From **Figure 7** it is clear that the low-temperature/high-strain-rate region and the high-temperature/moderate-strain-rate region do not facilitate deformation due to poor process stability and low power-dissipation efficiency. In the low left-hand corner or the upper right-hand corner, there is suitable process stability but the power-dissipation efficiency is only around 16 % and 25 %, respectively; the processability is also unfavorable. The ideal processing zone of the 1235 aluminum alloy exists in the high-temperature/low-strain-rate region due to better process stability and higher power-dissipation efficiency.

**4.4 TEM images under different deformation conditions**

The efficiency values of the hot-processing map exhibited in the domain are typical of the dynamic recrystallization process in the alloys. This was further confirmed on the basis of microstructure observations on the samples deformed under the conditions of the region.

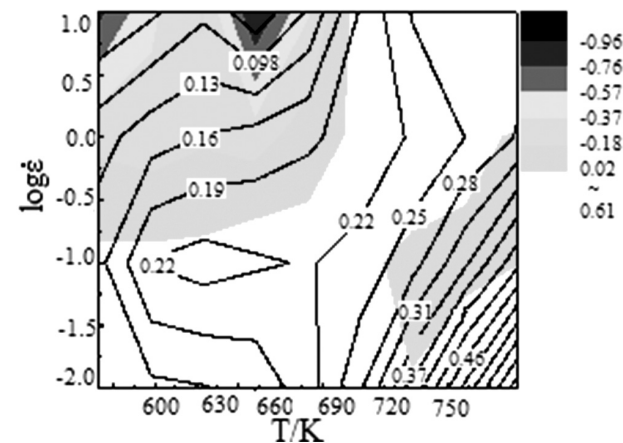


**Figure 7:** Hot-processing map of the 1235 aluminum alloy  
**Slika 7:** Načrt preoblikovanja v vročem za aluminijevo zlitino 1235

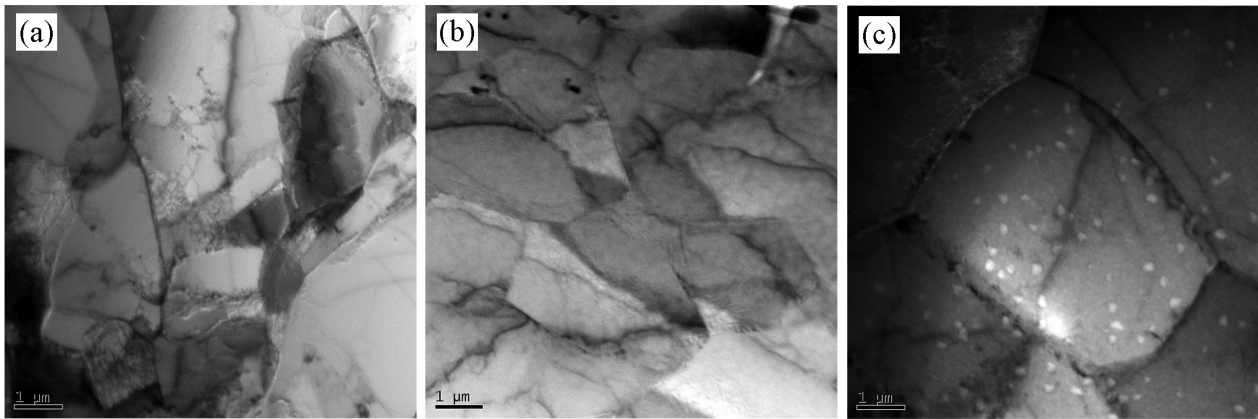


**Figure 8:** TEM images of the 1235 aluminum alloy at: a) 573 K,  $0.1 \text{ s}^{-1}$ , b) 673 K,  $10 \text{ s}^{-1}$  and c) 773 K,  $0.01 \text{ s}^{-1}$

**Slika 8:** TEM-posnetki aluminijeve zlitine 1235 pri: a) 573 K,  $0,1 \text{ s}^{-1}$ , b) 673 K,  $10 \text{ s}^{-1}$  in c) 773 K,  $0,01 \text{ s}^{-1}$

Typical microstructures obtained from the specimens at the temperatures of 573 K, 673 K and 773 K, and the strain rates of  $0.1 \text{ s}^{-1}$  and  $10 \text{ s}^{-1}$  are shown in **Figure 8**.

The characteristics of the grains in the 1235 aluminum alloy observed after hot deformation are shown to prove the reliability of the results of the hot-processing map. As seen in **Figure 8a**, the transgranular dislocation lines are concentrated, while the grain boundaries curve and become blurred due to dislocation tangling. In **Figure 8b** there are some elongated grains and small round grains in the microstructure; some grains cannot grow fully due to the high-strain rate. Judging from the appearances of the recrystal grains and grain boundaries, dynamic recrystallization has not been completed or there was only partial dynamic recrystallization accompanied by hardening as the 1235 aluminum alloy, hot deformed in these deformation conditions, tends towards instability. Thus, the processing performance is not satisfactory. At 773 K and  $0.01 \text{ s}^{-1}$ , a grain structure with integrity can be clearly seen on **Figure 8c**. Dynamic recrystallization has already grown fully producing rounded grains in the alloy. However, isometric recrystallized grains are in favor of the deformation processing by the deformation condition and show better mechanical properties. In consequence, the 1235 aluminum alloy has an ideal deformation mechanism of its microstructure at the high-temperature/low-strain rate, which is consistent with the result of the hot-processing map. It is better to try to avoid deformation at the low-temperature/high-strain rate or at the high-temperature/moderate-strain rate.

## 5 CONCLUSIONS

The power-dissipation map, the instability map, the hot-processing map and TEM images have been used to study the characteristics of the 1235 aluminum alloy after hot deformation. In the study the power-dissipation efficiency of the 1235 aluminum alloy increases from the low-temperature/high-strain-rate region to the high-tem-

perature/moderate-strain-rate region in the power-dissipation map. There are two instability regions in the hot-processing map of the 1235 aluminum alloy: one at the low-temperature/high-strain rate, another at the high-temperature/moderate-strain rate. It is better to avoid deformation in these two regions. The processing of the 1235 aluminum alloy is best in the high-temperature/low-strain-rate region and the power dissipation efficiency is around 46 %.

## Acknowledgements

The authors acknowledge, with gratitude, the financial support received from the Fujian Natural Science Foundation (E0610004) and the Technology Project of the Fujian Education Department (JA09262), China.

## 6 REFERENCES

- Y. V. R. K. Prasad, Processing maps: A Status Report, *Journal of Materials Engineering and Performance*, 12 (2003), 638–645
- Y. V. R. K. Prasad, T. Seshacharyulu, Processing maps for hot working of titanium alloys, *Materials Science and Engineering A*, 243 (1998), 82–88
- M. Zhou, D. Shu, L. Li, W. Y. Zhang, B. D. Sun, J. Wang, H. J. Ni, Performance improvement of industrial pure aluminum treated by stirring molten fluxes, *Materials Science and Engineering A*, 347 (2003), 280–290
- Y. V. R. K. Prasad, H. L. Gegel, S. M. Doraivelu, J. C. Malas, J. T. Morgan, K. A. Lark, D. R. Barker, Modeling of dynamic material behavior in hot deformation: Forging of Ti-6242, *Metallurgical and Materials Transaction A*, 15 (1984), 1883–1892
- Y. Liu, R. Hu, J. S. Li, H. C. Kou, H. W. Li, H. Chang, H. Z. Fu, Characterization of hot deformation behavior of haynes 230 by using processing maps, *Journal of Materials Processing Technology*, 209 (2009), 4020–4026
- Y. V. R. K. Prasad, Author's reply: Dynamic materials model: basis and principles, *Metallurgical and Materials Transaction A*, 27 (1996), 235–236
- J. Liu, Z. S. Cui, C. X. Li, Analysis of metal workability by integration of FEM and 3-D processing maps, *Journal of Materials Processing Technology*, 205 (2008), 497–505

- <sup>8</sup>G. S. Fu, W. Z. Chen, K. W. Qian, Effects of melt-treatment technique on the metallurgical quality and mechanical properties of Al sheet used for can manufacture, *Key Engineering Materials*, 297 (2005), 482–488
- <sup>9</sup>G. S. Fu, W. Z. Chen, K. W. Qian, Behavior of flow stress of aluminum sheets used for pressure can during compression at elevated temperature, *Acta Metallurgica Sinica*, 18 (2005), 756–763
- <sup>10</sup>Y. L. Chen, G. S. Fu, W. Z. Chen, Influence of melt-treatment on material constants of aluminum sheet used for easy-open can during hot deformation, *Transactions of Nonferrous Metals Society of China*, 16 (2006), 304–310
- <sup>11</sup>S. O. Poulsen, E. M. Lauridsen, A. Lyckegaard, J. Oddershede, C. Gundlach, C. Curfs, D. J. Jensen, In situ measurements of growth rates and grain-averaged activation energies of individual grains during recrystallization of 50 % cold-rolled aluminium, *Scripta Materialia*, 64 (2011), 1003–1006
- <sup>12</sup>B. Bozzini, E. Cerri, Numerical reliability of hot working processing maps, *Materials Science and Engineering A*, 328 (2002), 344–347